Experimental Investigation on the Ternary Phase Diagram Cu–Sn–P

Andreas Ludwig, Monika Grasser, Wolfram Schillinger

Although parts of the ternary system Cu–Sn–P especially in the Cu rich corner are already described in literature, the comparison of the experimental observations in the ternary system and the numerical assessment work shows some differences according the presence of some phases. Besides, the ternary eutectic point is of special interest for industry because the presence of the P rich phase Cu_3P, occurring at the ternary eutectic point, could influence the brittleness of the final bronze product. However, the presence of the ternary eutectic point and its position in the phase diagram are still questionable. Therefore, the basic aim of the presented experimental investigation is to describe and verify the known ternary system. The performed thermodynamic investigation includes numerical simulations of the binary systems CuSn and CuP and the ternary system Cu–Sn–P in the Cu rich corner and an experimental investigation containing differential thermal analysis and annealing experiments for the binary and ternary systems. In addition, the identification of the phases and phase regions is based on SEM and light microscope investigations.

Keywords:

Phosphor bronze – Phase diagram – Ternary eutectic point – Microstructure

Experimentelle Untersuchungen am ternären Phasendiagramm Cu–Sn–P

Obwohl die Cu-reiche Ecke des ternären Phasendiagramms Cu–Sn–P in der Literatur beschrieben wird, zeigt der Vergleich experimenteller Beobachtungen mit numerischen Phasendiagrammansätzen bezüglich des Auftretens einzelner Phasen Unterschiede. Darüber hinaus ist der ternär-eutektische Punkt von speziellem industriellem Interesse, da die P-reiche Cu_3P-Phase, die einen Bestandteil des ternären Eutektikums bildet, die Sprödigkeit des fertigen Bronzeprodukts beeinflusst. Dennoch ist die Existenz des ternär-eutektischen Punktes bzw. dessen Lage immer noch umstritten. Daher ist das grundlegende Ziel der vorliegenden experimentellen Untersuchung, das Auftreten und die Existenzbereiche der einzelnen Phasen zu untersuchen, und somit das bekannte Cu–Sn–P-Phasendiagramm zu verifizieren. Neben experimentellen Untersuchungen mittels Differentialthermoanalyse (DTA), Langzeit- Diffusionsglühexperimenten von binären und ternären Proben und elektronen- und lichtmikroskopischen Untersuchungen zur Phasenidentifizierung wurden die auftretenden Phasen in den binären Randsystemen CuSn und CuP sowie in der Cu-reichen Ecke des ternären System Cu–Sn–P numerisch simuliert und mit den experimentellen Beobachtungen verglichen.

Schlüsselwörter:

Phosphorbronze – Phasendiagramm – Ternär-eutektischer Punkt – Gefüge

Investigation expérimentale du diagramme de phase ternaire Cu–Sn–P

Investigación experimental sobre el diagrama de fase ternario Cu–Sn–P

Paper presented on the occasion of the Copper 2010 Conference held June 6 to 10, 2010 in Hamburg, Germany.

This is a peer-reviewed article.

1 Introduction

According to European standards the Sn-content in bronze is limited to 9 wt.-% Sn in wrought alloys and to 13 wt.-% in cast alloys. In the as-cast state, the microstructure of bronze consists of α-phase (α) and the eutectoid of the α- and δ-phase (δ). The large solidification interval is one of the reasons for the strong macrosegregation often observed in bronze castings. In addition, diffusion of Sn in the solid is rather small, which is the reason that one cannot use heat treatment to get rid of already formed segregations. The δ-phase, forming due to solid-solid transformation during cooling, is rather rigid but present as interdendritic precipitate which leads to inhomogeneities in the solidified material.

Most of the fundamental research related to bronze has been performed many years ago [1-3]. During the last decades the improvement of experimental methods, and with that of measurement accuracy, was remarkable. However, only little experimental work has been performed on the thermodynamics of the system Cu–Sn–P, thought to represent the thermo-dynamic behaviour of common technical bronze alloys. Already published phase diagrams and assessment work for the binary systems Cu–Sn and Cu–P [4-7] are based on experimental observations of the 1930's to the 1980's. Therefore, it makes sense to validate those results with present measurement methods.

The ternary system itself was assessed by [7] by taking major publications on the binary and one experimental study on the ternary system [8] into account. Figure 1 shows two isopleths at 5 wt.-% P to compare (a) the experimental work [8] and (b) the calculated values based on the assessment work of [7]. Based on the binary phase diagrams γ is included in the numerical assessment although it was not observed in the experimental study of [8]. The circle marks in both plots the region close to the ternary eutectic point which is still under discussion [4]. The existence of a ternary eutectic point at CuSn14.8P4.5 mass-% was proposed in several publications from 1910 to 1937. Other authors (e.g. [3, 9]) suggested that this "ternary eutectic" should rather be a transition reaction L + α → β + Cu$_3$P. This was also concluded in the experimental study of [8] (Figure 1a).

The numerical thermodynamic simulation of the software Thermo-Calc is based on the CALPHAD (Calculation of Phase Diagrams) approach. A database was implemented for the Cu–Sn–P system in the Cu rich corner by Thermo-Calc ([11-12], mainly based on [7]). The presented thermodynamic investigation includes numerical simulations of the binary systems Cu–Sn and Cu–P and the ternary system CuSnP in the Cu rich corner, whereas the experimental investigation is based on DTA measurements and annealing experiments, investigated by microscope and microprobe.

2 Computational thermodynamics

The calculated binary Cu-Sn (a) and Cu-P (b) phase diagrams are displayed in Figure 2. It has to be mentioned that in comparison to the already published phase diagrams [5, 6] there are some differences, especially in the curvature of the liquidus line for both systems. In addition, phase δ, ε, and ξ are treated as compounds in the calculation whereas they have a certain solubility range in previous literature [7]. For details about the comparison between already published and calculated data the reader is referred to [12]. Summarizing it can be stated that the deviations are in an acceptable range for the ongoing study.

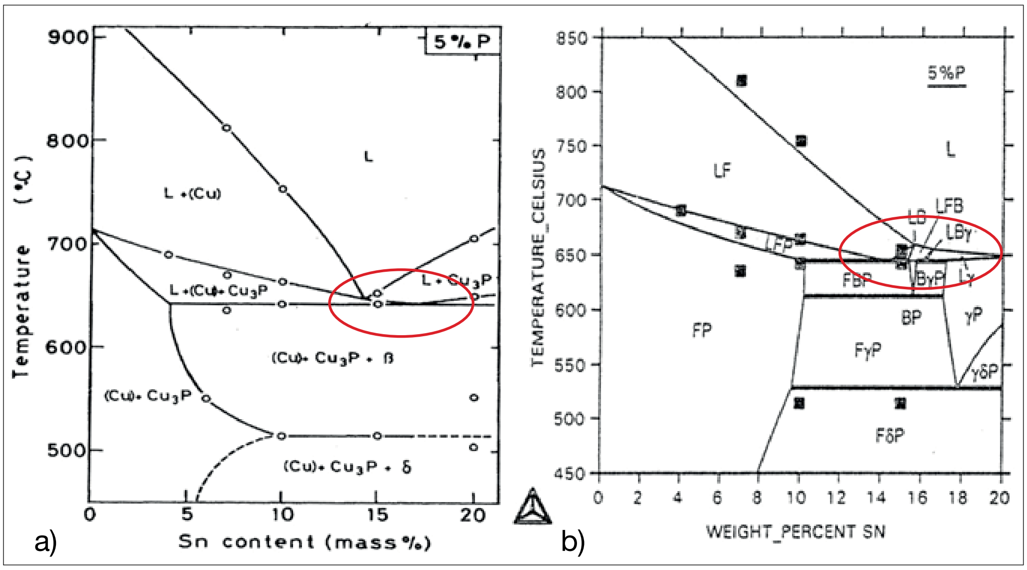

Fig. 1:
Vertical section (isopleth) of the ternary phase diagram Cu–Sn–P at 5 wt.-% P: (a) based on the experimental investigation of [8]. Displayed points show DTA (Differential Thermal Analysis) measurements ((Cu) = α), and the lines show the interpolated expected phase regions [8]; (b) based on the numerical assessment work performed by [7]. The displayed dark small squares show DTA measurements [18] and the lines show the calculated phase diagram (F = α, P = Cu$_3$P, B = β) [7]. The two phase regions LB and LFB in (b) have to be changed to LFB for LB and LB for LFB. Circles indicate the area close to the ternary eutectic point of the system.

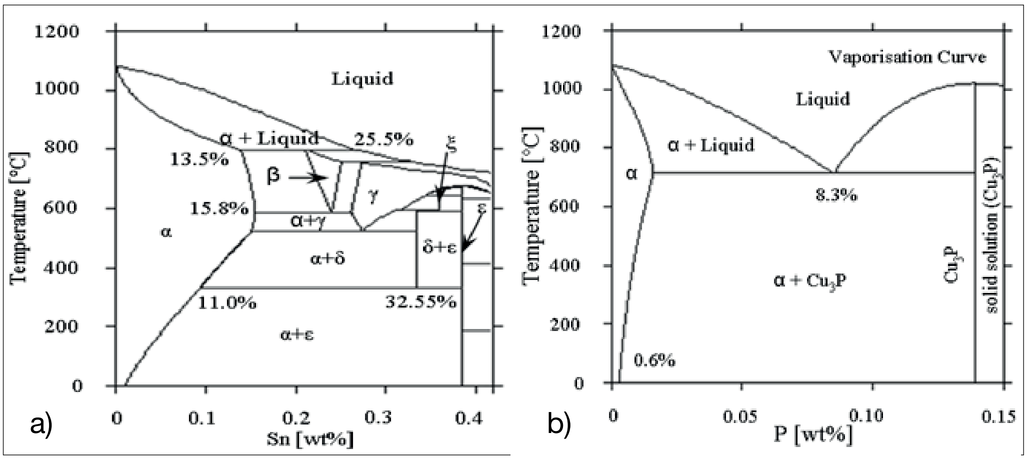

Fig. 2:
(a) Phase diagram for Cu–Sn, (b) Phase diagram of Cu–P calculated with Thermo-Calc (database CuSnII). α = Cu (max. Sn 15.8 wt.-%); β ~ Cu$_{17}$Sn$_3$; γ ~ Cu$_3$Sn; δ ~ Cu$_{41}$Sn$_{11}$; ε ~ Cu$_3$Sn; ξ ~ Cu$_{10}$Sn$_3$ (nomenclation taken from [4]).

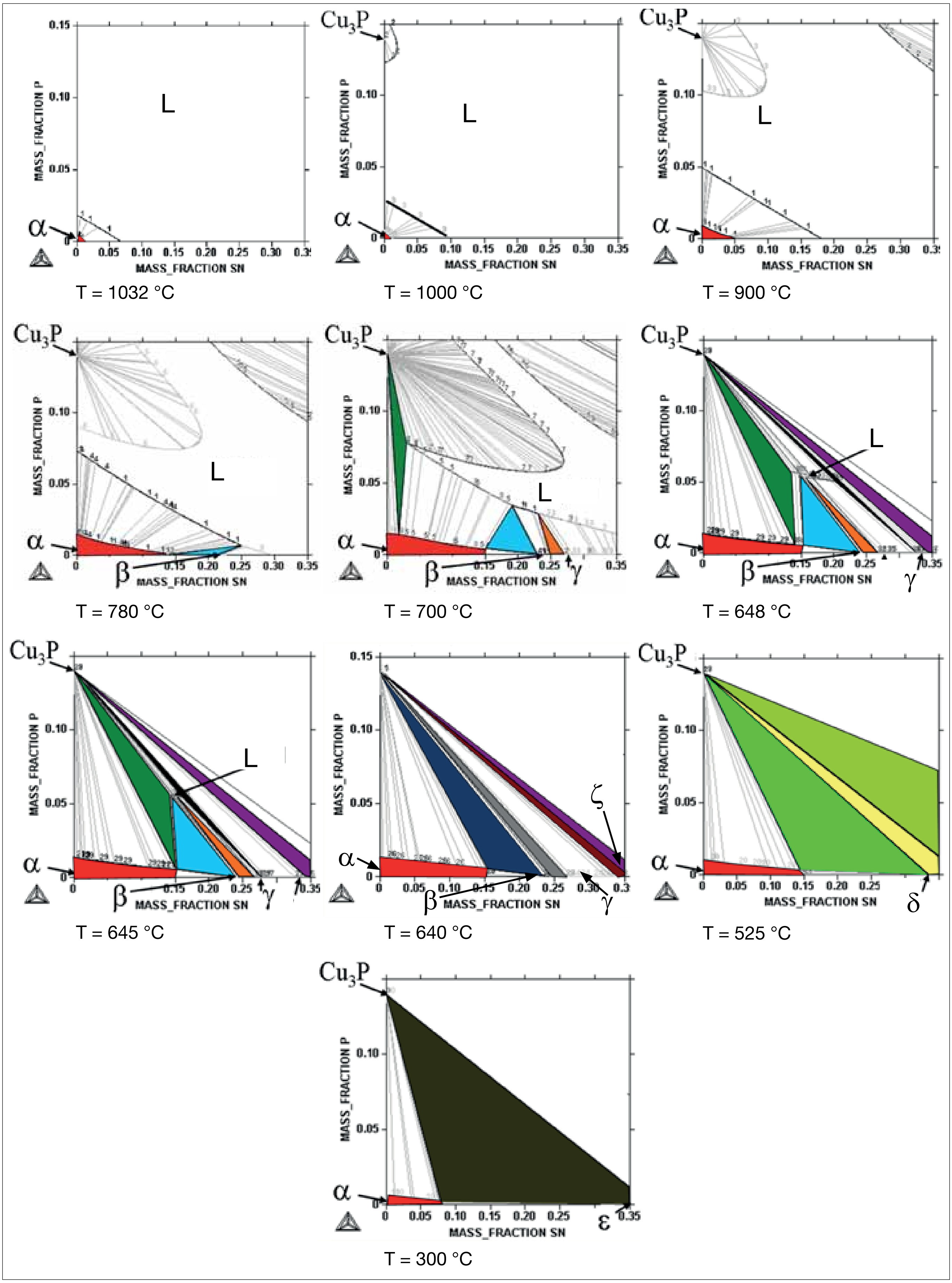

Fig. 3: The presented isothermal sections of the ternary phase diagram of Cu–Sn–P in the Cu rich corner are calculated with Thermo-Calc (database CuSnII). α = Cu (max. Sn 15.8 wt.-%, P 2 wt.-%); β ~ $Cu_{17}Sn_3$; γ ~ Cu_3Sn; δ ~ $Cu_{41}Sn_{11}$; ε ~ Cu_3Sn; ξ ~ $Cu_{10}Sn_3$ (nomenclation taken from [4]).

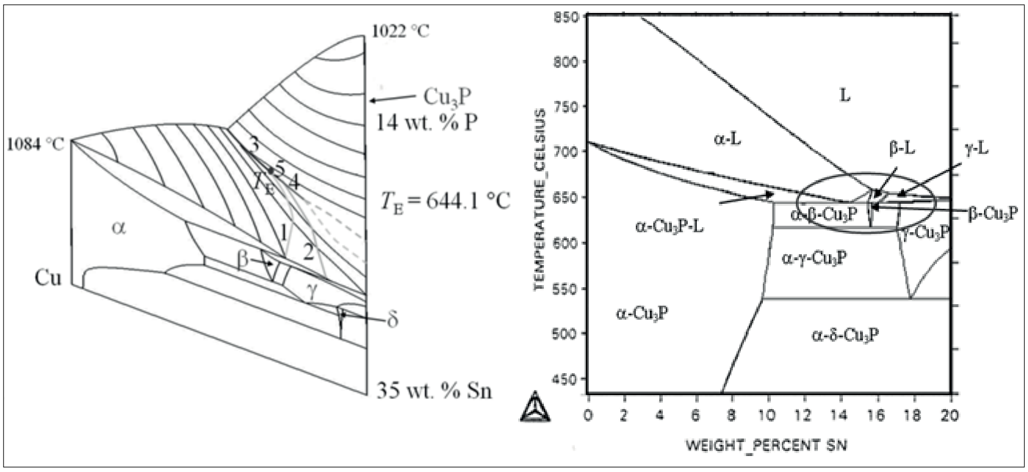

Fig. 4:
(a) 3D liquidus surface of the Cu rich corner of Cu–Sn–P is displayed up to 35 wt.-% Sn and 14 wt.-% P.
(b) Calculated isopleth for the same P concentration as displayed in Figure 1. Calculated with Thermo-Calc (database CuSnII).

Figure 3 shows isothermal sections of the ternary Cu–Sn–P system for T = 1032, 1000, 900, 780, 700, 648, 645, 640, 525, and 300 °C. The CuSnII database is restricted to the Cu rich corner up to 15 wt.-% P and about 40 wt.-% Sn. Therefore the sections are calculated within this limitation.

Starting with 100 % liquid (L), the α-phase forms after the melting point of Cu, T_{lCu} = 1085 °C is reached (Figure 3, T = 1032 °C). Below the melting point of the compound Cu_3P (appears as a point in the isothermal sections) T_{lCu3P} = 1022 °C, the two phase region Cu_3P–L is present in the isothermal section (Figure 3, T = 1000 °C). With decreasing temperature the one phase region of α and the two phase regions of α–L and Cu_3P–L are increasing (Figure 3, T = 900 °C).

In the isothermal section at T = 780 °C, β is present as a result of the peritectic reaction L + α → β starting at T = 799 °C. With solidification of the third phase, the three phase region α–β–L (Figure 3, T = 780 °C) can be observed. In the isothermal section at T = 700 °C, γ is occurring as a result of the peritectic reaction L + b → γ at T = 756 °C, and the three phase region β–γ–L appears. Besides, the eutectic groove between a and Cu_3P is reached and the three phase region α–Cu_3P–L is visible (Figure 3, T = 700 °C). Further cooling leads to a decrease of the L region to a small area at T = 648 °C. At slightly lower temperature, namely at approximately T = 644 °C, the ternary eutectic point is reached at a concentration of 15 wt.-% Sn and 5.5 wt.-% P (number T_E, Figure 4a).

At T = 648 °C the decrease of the liquid phase leads to the presence of two more three phase regions, namely Cu_3P–γ–L and Cu_3P–ε–γ. The ε-phase (ε) is located at ~38 wt.-% Sn in the binary phase diagram and therefore its one phase region (appearing as a point in the isothermal section) is not visible in the presented ternary sections. In the isothermal section at T = 640°C the ξ-phase (ξ) occurs in the three phase region Cu_3P–γ–ξ as a result of the peritectoid reaction ε + γ → ξ. Since x has a Sn content of approximately 36 wt.-% Sn the one phase region of the binary system is also not visible in the ternary sections.

The liquid phase has already disappeared at T = 640 °C and four three phase regions are present, namely Cu_3P–ε–ξ, Cu_3P–γ–ξ, Cu_3P–β–γ, and Cu_3P–α–β. At T = 525 °C the δ-phase (δ) has already appeared while ξ disappeared as a result of the peritectoid reaction ξ + γ → δ. In this section the three phase regions of Cu_3P–δ–ε, and Cu_3P–α–δ are present. With further cooling only the solubility of Sn in α is decreasing and therefore at T = 400 °C the same phases are stable as at T = 525 °C. Further decrease in temperature leads to the eutectoid reaction δ → α + ε at T ~ 350 °C and therefore δ is not present in the isothermal section at T = 300 °C. At this temperature the phase regions of Cu_3P, α and ε are connected by the three phase region Cu_3P–ε–α.

The liquidus surface is redrawn based on calculations performed with Thermo-Calc and displayed in Figure 4a. Here the black lines define the isotherms and the numbered lines the mono variant lines (1) for the peritectic reaction L + α → β + L (2) for the peritectic reaction L + β → γ + L, and (3) for the eutectic reaction L → Cu_3P + α + L which ends in the ternary eutectic point (T_E). (4) represents the monovariant line of the eutectic reaction L → Cu_3P + γ + L and attached to it (5) shows the one of the eutectic reaction L → Cu_3P + β + L which ends again in the ternary eutectic point (T_E). The last plot in Figure 4b displays the vertical section (isopleth) at 5 wt.-% P of the ternary phase diagram calculated with database CuSn1. The area marked with the circle corresponds to the area also marked in the presented isopleths in Figure 1.

3 Experimental description

The samples for the annealing experiments have been prepared by Wieland Werke AG. Figure 5 shows micrographs as example for three used alloys: (a) for CuSn20 containing α and δ eutectoid, (b) for CuP8.3 showing α and Cu_3P eutectic, and (c) for the ternary alloy CuSn11P5 after the sample preparation (the concentrations are nominal concentrations). The samples have been taken as cast after the sample preparation. The actual process of the sample preparation and the displayed microstructure is not discussed here in detail because it is beyond the scope of this work.

The sample preparation for the diffusion experiments performed is described in detail in [12]. Therefore only some information is given here. Figure 6a shows the test arrangement containing the furnace, the used digital multimeter and the position of the sample during annealing

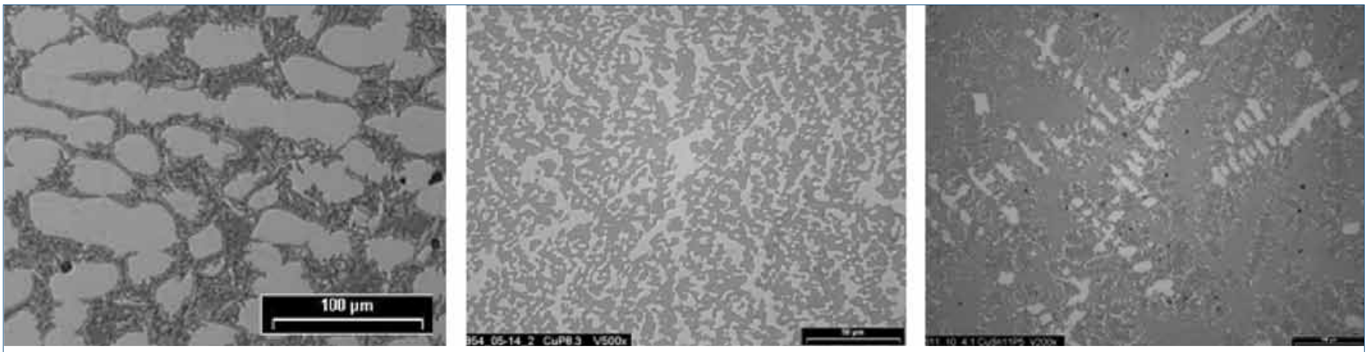

a) CuSn20 b) CuP8.3 c) CuSn11P5

Fig. 5: Micrographs of (a) CuSn20, (b) CuP8.3, (c) CuSn11P5 as cast

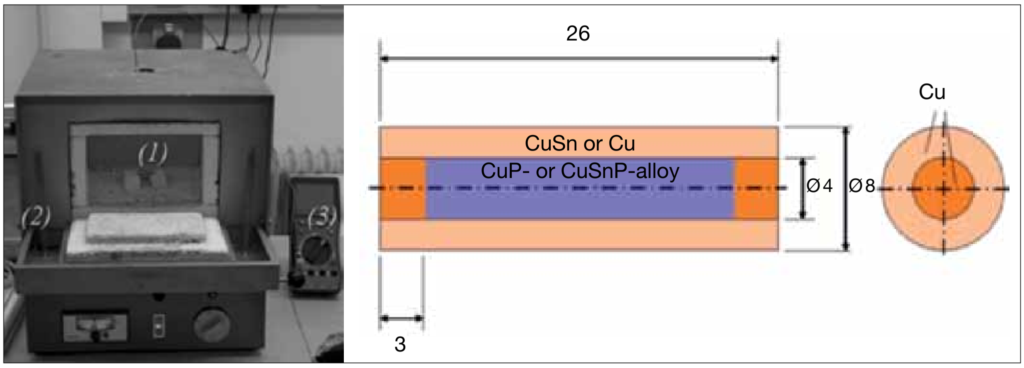

Fig. 6:
(a) Test arrangement consisting of (1) the sample, (2) the furnace and (3) the digital multimeter. (b) Cylindrical geometry applied for the diffusion experiments is shown. The outer tube consists of Cu or CuSn and the inner cylinder of CuSnP or CuP. Cu pieces at the top and the bottom close the sample. Dimensions in [mm].

[12]. According to test measurements, the furnace holds the temperature with a deviation of $\Delta T = \pm 1$ °C. Radial symmetrical diffusion is approximated by an axis symmetric geometry as schematically demonstrated in Figure 6b. Since P tends to evaporate, a cylindrical geometry is used consisting of an outer tube (about 2 mm extension and a radius of about 8 mm) of Cu or Cu–Sn and of a core made of Cu–P or Cu–Sn–P. In addition, the sample was closed at the top and at the bottom by Cu pieces as displayed (Figure 6) to avoid evaporation of P. After annealing the samples were quenched in cold water.

4 Results and discussion

DSC measurements have been performed for the binary systems as published in [12]. There it is indicated that the phase transition temperatures are close to the ones proposed by [5] and calculated with Thermo-Calc (database CuSnII) [12]. Since the γ- and ε-phase were not observed in former studies, additionally, several binary samples have been annealed and the observed phase distribution was compared with the one published by [5] and calculated with the database CuSnII. Figure 7 shows three micrographs as example for the performed work: (a) CuSn20 after annealing at 650 °C for 3 days, (b) CuSn35 and (c) CuSn37 after annealing at 400 °C for 21 days. The microstructure of the sample (a) CuSn20 shows the α-phase in equilibrium with the β-phase. In the SEM picture of the sample (b) CuSn35 the α- and δ-phase are observed and in the one of CuSn37 the δ- and ε-phase are present in equilibrium.

By comparing these phase distributions with the phase diagram displayed in Figure 2 it can be seen that the experimentally observed phase distributions agree with the one proposed by [5]. Although, ε was not observed forming by solid-solid transformation out of the α+δ-eutectoid, it is forming directly out of the melt in samples with high Sn concentration (e.g. CuSn37).

Besides, a diffusion experiment, for a combination of CuSn20 and CuP8.3, at the annealing temperature of

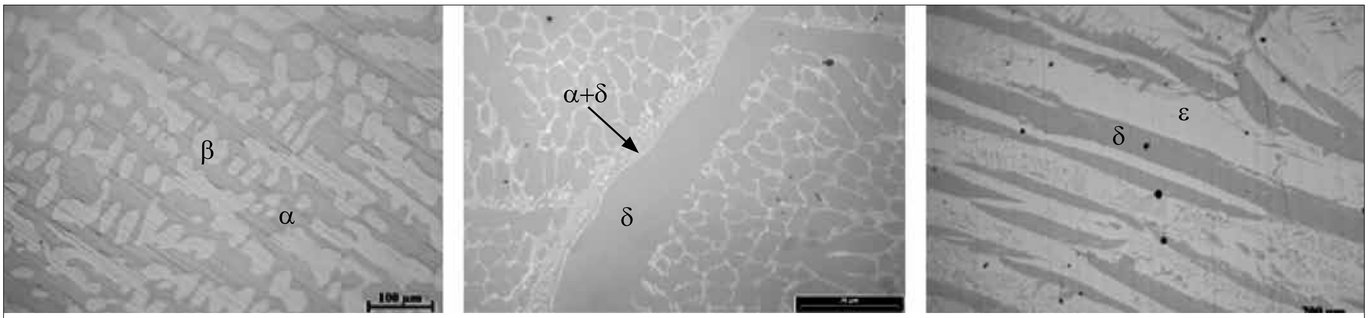

a) CuSn20, 650 °C, 3 days b) CuSn35, 400 °C, 21 days c) CuSn37, 400 °C, 21 days

Fig. 7: Micrographs of (a) CuSn20; (b) CuSn37; (c) CuSn35

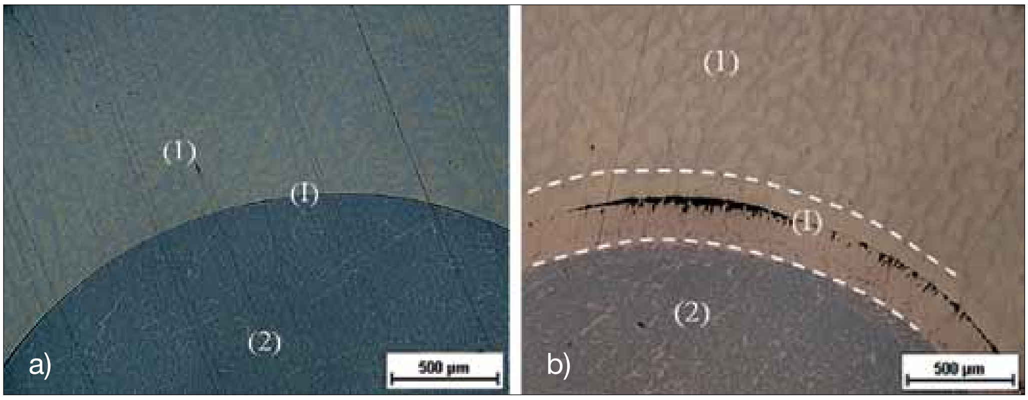

Fig. 8:
Micrograph before (a) and after (b) annealing at 648 °C and following quenching. (1) CuSn20 tube showing (a) α-δ-eutectoid and b) α-β-peritectic, (2) CuP8.3 cylinder consisting of Cu_3P-α-eutectic in (a) and (b), and (I) is the contact area between the two samples with pores. White broken line indicates the Sn and P depleted region.

648 °C was performed for three days. After annealing, the sample was quenched in cold water and prepared for further measurements. SEM and microscopy was applied for phase detection.

Figure 8 shows a micrograph of the annealing sample CuSn20–CuP8.3 before and after annealing and quenching. The outer tube consists of α-δ-eutectoid ((1), a) and the cylinder in the middle of α-Cu_3P-eutectic ((2), a) where the compound Cu_3P appears as a fine dispersed gray phase. According to the binary phase diagram these two phases are forming Cu_3P-α-eutectic. In Figure 4b the inner cylinder still shows Cu_3P-α-eutectic after annealing and quenching. However, the microstructure, especially in the outer tube, has changed due to the formation of α-β-peritectic. At the contact interface, both, the Cu_3P-α-eutectic and α-β-peritectic are not visible any more (I). Diffusion is observed at the sample boundary, which takes place in the area which is marked by the white broken lines. In this region Sn and P are solved in the α-phase (up to 15 wt.-% Sn and 2 wt.-% P).

Figure 9a shows the concentration measurements performed for Sn (dark gray) and P (light gray) at the diffusion interface of this sample whereas in Figure 9b a micrograph of the binary diffusion sample in the diffusion area is shown. The red broken lines mark the boundaries between the two and one phase regions whereas the white broken line indicates the expected boundary between the diffusion partners. It can be seen that the Sn concentration shows a smooth distribution whereas the P concentration reveals big jumps because a is resolving just max. 2 wt.-% P

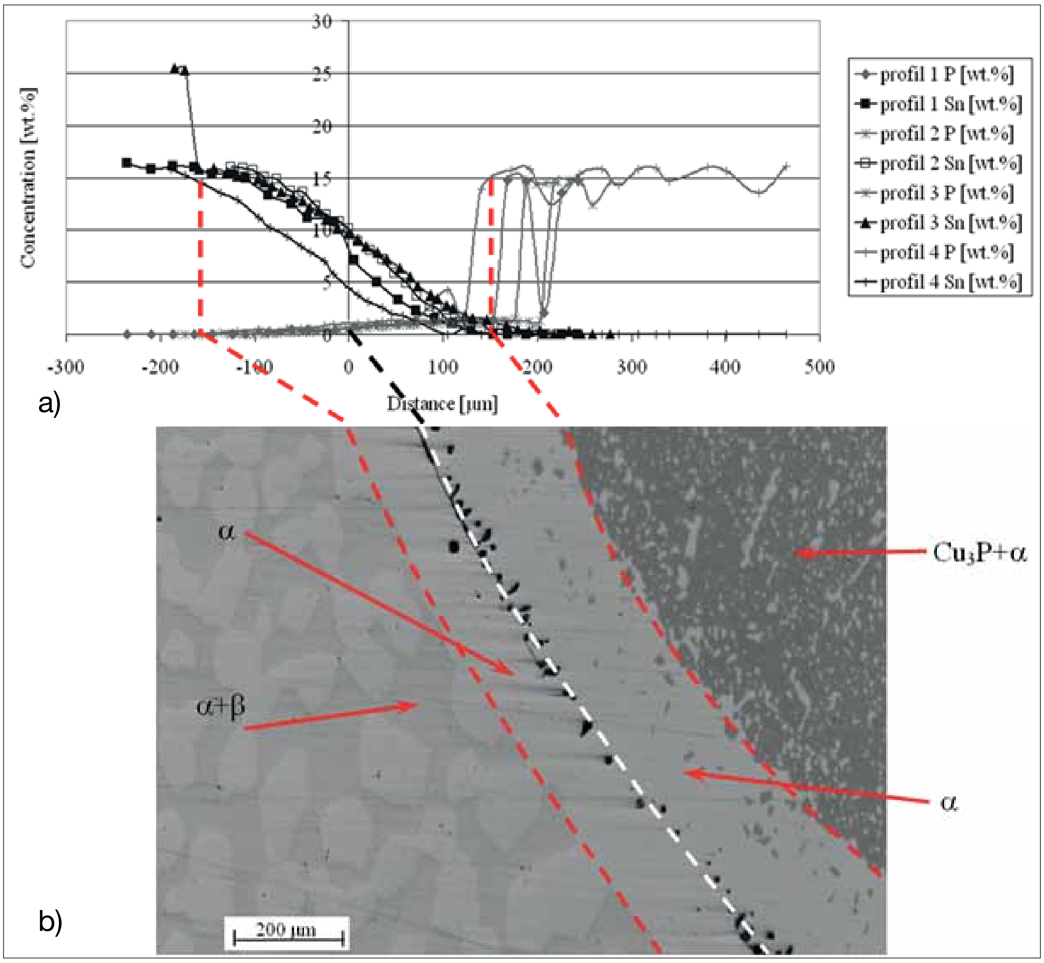

Fig. 9:
(a) Concentration measurements in the binary diffusion sample for Sn (dark gray) and P (bright gray) at the diffusion interface. (b) SEM picture of the binary diffusion sample in the diffusion area.

whereas Cu$_3$P has around 14 wt. % P. The red broken lines correlate the depth of diffusion according the SEM investigations with the observed microscopic structure change in this area.

After annealing, the samples are connected at the interface although a certain amount of pores is still present. The jumps in the detected concentrations in both, the CuSn and CuP sample, are caused by the fact that the measurement series has been performed as point measurement and therefore sometimes the Sn and P rich phases themselves are detected. The low P content detected in α corresponds to its solubility according to the shown phase diagrams. It seems that this low solubility slows the diffusion of P down towards the boundary and leads to diffusion towards the centre of the CuP sample where more Cu$_3$P is built. Here higher P concentrations, in comparison to the reference sample, are detected.

Based on the SEM measurements rough diffusion coefficients are estimated for the temperature of 648 °C according to the measured profiles for Sn in the α region with about $D_{Sn\alpha} \sim 10^{-13}\ m^2 \cdot s^{-1}$ and for P in the α region with about $D_{P\alpha} \sim 3 \cdot 10^{-14}\ m^2 \cdot s^{-1}$. The value observed for Sn lies in a range as proposed by literature for binary CuSn diffusion. For P just a diffusion coefficient for impurities is available in literature, therefore no comparison is possible for the diffusion of P in Cu with 8.3 wt.-% P.

Phase distribution, concentrations and phase regions of some defined ternary samples have been studied by analysing unannealed as well as annealed samples. The observed phase distribution was compared with the ternary phase diagram calculated with the database CuSnII. Figure 10 displays three micrographs of ternary samples before annealing and the detected phases by SEM investigations, namely of (a) CuSn30P1 (nominal concentration) showing δ-dendrites surrounded by a δ-Cu$_3$P two phase region, (b) CuSn17P2 consisting of α-dendrites and two phase regions of α–δ and α–Cu$_3$P and (c) CuSn11P5 showing α-dendrites, α–Cu$_3$P two phase regions and α–δ–Cu$_3$P three phase regions. Further interpretation of the history of the observed phase distribution is not done here. Figure 11 shows the same samples after annealing and quenching. All three samples have been annealed at 640 °C (a) CuSn30P1 for 24 hours, (b) CuSn17P2 and (c) CuSn11P5 for 42 hours.

Figure 12 shows an isothermal section of the ternary system at 640 °C for comparison with the proposed thermodynamics, the black squares mark the sample concentrations. Based on the performed investigations, a two phase region of γ + Cu$_3$P is detected in sample CuSn30P1. Sample CuSn17P2 has a microstructure containing three phases, namely α, β and Cu$_3$P. The third sample, CuSn11P5 shows also the same three phases after annealing. Comparing the detected phase distributions with the proposed ones by computational thermodynamics, it can be stated that good agreement is observed. One special feature is the detection of the γ- and β-phase after quenching at room temperature. Although the γ-phase was not detected by the experimental work performed by [8] (Figure 1, dark small squares), [7] included the γ-phase in his assessment work for the ternary phase diagram calculation. γ is thought to evolve from β during cooling by keeping the fcc structure as β does. Further cooling leads then to the eutectoid transition

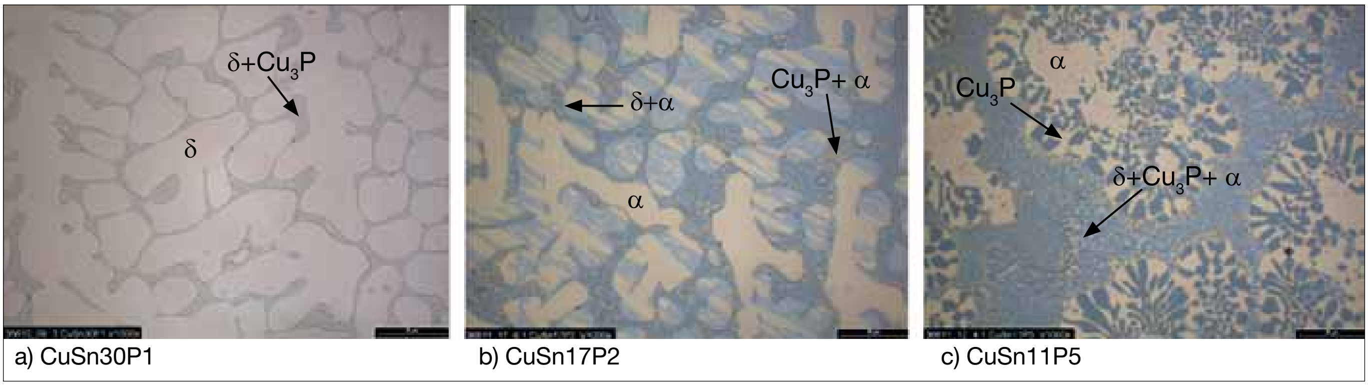

a) CuSn30P1
b) CuSn17P2
c) CuSn11P5

Fig. 10: Micrographs (a) CuSn30P1; (b) CuSn17P2; (c) CuSn11P5

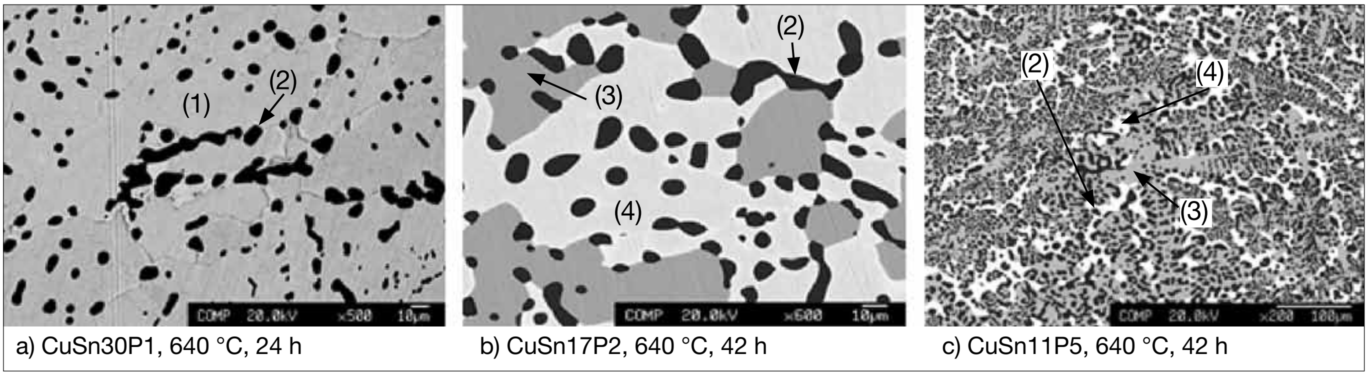

a) CuSn30P1, 640 °C, 24 h
b) CuSn17P2, 640 °C, 42 h
c) CuSn11P5, 640 °C, 42 h

Fig. 11: SEM pictures (a) CuSn30P1; (b) CuSn17P2; (c) CuSn11P5. Phases labelled with (1) γ (gray), (2) Cu$_3$P (black), (3) α (dark gray), (4) β (bright gray to white).

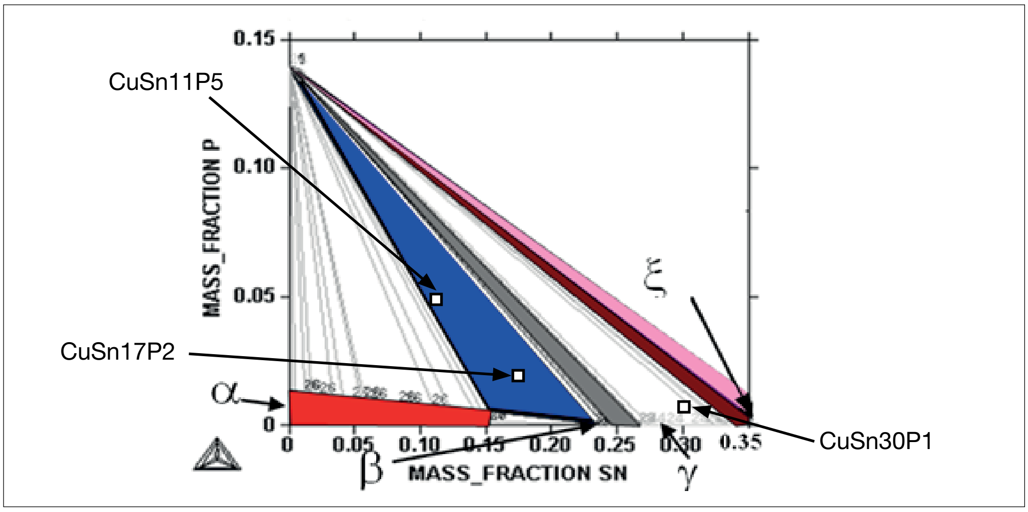

Fig. 12:
Isothermal section at 640 °C, mass fraction Sn up to 0.35, mass fraction P up to 0.15. The black squares mark the position of the annealed sample concentrations.

of γ at 520 °C to α + δ [5]. After [2], neither β nor γ can be observed after quenching at room temperature, here metastable transition states are observed that show sometimes martensitic structure. But, according to the recent experimental study the γ-phase is present in the ternary phase diagram at expected higher Sn concentrations as already proposed by [7] in his assessment work.

However, applying etching to samples situated in regions containing the γ phase shows some kind of transformation going on. This can be seen in Figure 13, where two samples, each with a concentration of CuSn20P6, annealed at 642 °C and 640 °C for 20 days, are displayed after annealing, quenching and etching. Figure 13a displays an area where, before etching, the two phase region β-Cu_3P seemed to be stable. Although the microstructure in the centre of the sample seemed to consist of just two phases, etching lead to observations in the SEM that illustrate the complex microstructure of this sample. The visible microstructure in Figure 13a shows that β (1) seems to transform to a brighter needle-like structure (2), especially at the boundary around Cu_3P (black big regions). Here, it is visible that either a third phase, which could be γ according to obtained Sn content, has been formed or a transition occurs appearing as a very fine, needle-like structure. However, it has to be kept in mind, that the gray scale difference, as well as the structure of the different phases is strengthened by etching. Attached to the Cu_3P "grain", visible at the left hand side of Figure 13b, also a region with a needle like structure ((2), 25.5 wt.-% Sn and 0.7 wt.-% P) is observed. This could indicate that in this area α-phase starts to form and one could think, that the bright needles are forming δ. In this case the detected Sn concentration could be underestimated by the SEM measurements due to the fact that a limit of about 1 µm is expected for the microprobe measurements. Therefore it could be a region that transforms to α-δ-eutectoid out of either γ or β. However, the detected Sn content induces the possibility that this is γ. The slightly darker region has a more or less uniform matrix and has a slightly lower Sn concentration than the surrounding regions ((1), 24 wt.-% Sn) and no remarkable P content why it is thought to be β. According to the phase diagram these samples are situated at or just above of the eutectic plane. Thermodynamics proposes for both samples the three phase region β–γ–Cu_3P for the detected concentrations.

To gain more information about this specific system additionally diffusion experiments and DSC/DTA measurements have been performed for the ternary samples which are the purpose of further studies.

5 Conclusions

The presented study includes a comparison of the numerical description of the ternary phase diagram Cu–Sn–P in the Cu rich corner based on calculations using database CuSnII and Thermo-Calc, annealing and diffusion experiments. The phase detection is based on microscopy and SEM investigations.

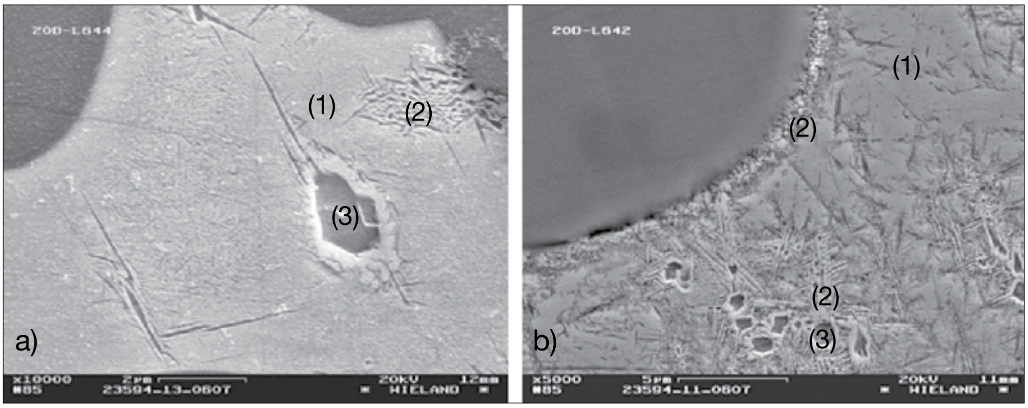

Fig. 13:
SEM picture after annealing of CuSn20P6 (a) at 642 °C, and (b) at 640 °C for 20 days, quenching and etching. (1) β (bright gray), (2) transformation area, (3) α (dark gray).

The experimental observations show good agreement with the proposed ternary phase diagram of [7]. The detection of γ in the ternary sample CuSn30P1 and in the two samples of CuSn20P6 after annealing at 640 °C and 642 °C is in good agreement with the thermodynamic calculations but controversy to the absence of γ in the DTA measurements of [18]. Here further investigations are ongoing for more information about the conditions of the appearance of the γ-phase.

In addition, ε was detected in binary samples with high Sn contents as proposed by thermodynamic data of [5] or [7]. In this case it seems that ε is stable when forming out of the melt in a Sn rich melt (CuSn37), also at room temperature. However, it was never observed in the present studies forming due to annealing in a temperature range of 400 °C due to solid-solid transformation which is in good agreement with literature [1, 2]. Therefore the recent study confirms that the formation of the ε-phase can be ignored for industrial processes.

Acknowledgement

This work is financially supported by the Austrian Christian-Doppler Research Society and Wieland Werke, Vöhringen, for which the authors kindly acknowledge. Besides we want to thank Professor J. Ågren (KTH) for the scientific support and for the possibility of SEM investigations at the “Chair of Mineralogy and Petrology” at the University of Leoben.

References

[1] Dies, K. (1967): Kupfer und Kupferlegierungen in der Technik. – Springer Verlag.

[2] Schumann, H. (1990): Dt. Verlag für Grundstoffind., Leipzig, neubearb. Aufl.13, 504-576.

[3] Verö, J. (1953): Zeitschrift anorg. allgem. Chemie, **213**, 257-272.

[4] Effenberg, G. & Ilyenko, S. (2007): Landolt-Börnstein-Group IV Physical Chemisty, 355-367.

[5] Massalsky, T.B. et al. (1986): American Society for Metals, 1.

[6] Massalsky, T.B. (Ed.) (1990): ASM International.

[7] Miettinen, J. (2001): Calphad, 25, 1, 67-78.

[8] Takemoto, T., Okamoto, I. & Matusumura, J. (1987): Trans. JWRI **16**, 301, 73-79.

[9] Levi-Malvano, M.L. & Orofino F.S. (1911): Gazz. Chim. Ital., **41**, 11, 269-297.

[10] SGTE (2003): Thermo-Calc.

[11] Thermo-Calc (2005): “CuSnII Database“, personal communication.

[12] Grasser, M., Mayer, F. & Ludwig, A. (2009): Thermodynamic Description of the System Cu–Sn–P – Computational Thermodynamics and Experimental Investigation on the Systems CuSn and CuP, conference proceedings, a publication of TMS, 47-54.

Prof. Dr. rer.nat. Andreas Ludwig
Christian-Doppler Laboratory for Multiphase Modeling
of Metallurgical Processes
Dept. of Metallurgy, University of Leoben
A-8700 Austria
smmp@unileoben.ac.at

Prof. DI Dr.mont. Monika Grasser
HTBLVA Ferlach
Schulhausgasse 10
9170 Ferlach
Austria
monika.grasser@htl-ferlach.at

Dr.-Ing. Wolfram Schillinger
Wieland Werke AG Ulm
Vöhringen
Germany